




Ferroelectrically induced half-metallicity, giant tunnel electroresistance, and giant tunnel magnetoresistance in spin-semiconducting LaBr₂

Xiaohong Zheng ^{1,*}, Zhifan Zheng,¹ Shili Yang,¹ Chun-Sheng Liu,² Lei Zhang ^{3,4} and Hua Hao ^{5,†}

¹College of Information Science and Technology, Nanjing Forestry University, Nanjing 210037, China

²College of Electronic and Optical Engineering, Nanjing University of Posts and Telecommunications, Nanjing 210023, China

³State Key Laboratory of Quantum Optics and Quantum Optics Devices, Institute of Laser Spectroscopy, Shanxi University, Taiyuan 030006, China

⁴Collaborative Innovation Center of Extreme Optics, Shanxi University, Taiyuan 030006, China

⁵School of Physics, Hangzhou Normal University, Hangzhou 311121, China



(Received 14 August 2024; revised 5 September 2024; accepted 12 September 2024; published 30 September 2024)

Half-metallicity is very important in spintronics due to its ability to realize fully spin polarized transport. Due to the rise of two-dimensional (2D) materials, how to achieve half-metallicity in 2D materials has attracted great attention in recent years and various schemes have been proposed for this goal in intrinsically non-half-metallic magnetic systems, whereas these schemes are primarily limited to antiferromagnetic systems. It is desirable and significant to turn ferromagnets into half-metals. In this work, by taking magnetic LaBr₂ monolayer as an example, based on density functional theory calculations, we propose a scheme to achieve half-metallicity in a kind of ferromagnetic systems called spin semiconductors by forming a van der Waals (vdW) heterostructure with a 2D ferroelectric material α -In₂Se₃. It is found that not only half-metallicity can be achieved in LaBr₂, but it can also switch between half-metal and semiconductor accompanying with ferroelectric polarization reversal under the external electric field. The switching is interpreted by the interlayer charge transfer due to the appropriate work function differences between the contacted two surfaces. Further the obtained extremely high spin polarization (99.94%), tunnel electroresistance ratio ($2.11 \times 10^5\%$), and tunnel magnetoresistance ratio ($1.62 \times 10^4\%$) in the subsequent transport study of the multiferroic tunnel junction constructed with LaBr₂/ α -In₂Se₃ vdW heterostructure demonstrates that this provides a novel scheme for the new multifunctional applications of spin semiconductors such as LaBr₂, either as a spin filter generator, or as a building block of data storage units based on giant tunnel electroresistance effect or giant tunnel magnetoresistance effect.

DOI: [10.1103/PhysRevB.110.115439](https://doi.org/10.1103/PhysRevB.110.115439)

I. INTRODUCTION

Since the discovery of giant magnetoresistance (GMR) in magnetic tunnel junctions in the late 1980s [1,2], the spin degree of freedom of electrons started to play a very important role in data storage, which led to the naissance of spintronics and greatly increased the storage density of memory devices [3–9]. The central goal of spintronics is to attain high spin polarization, and especially half-metallicity [10], which means 100% spin polarization is greatly desired. In terms of band structure, half-metallicity is characterized by a single spin channel crossing the Fermi level, with the other spin channel far from it [11–13]. For a material to be half-metallic, a prerequisite is that it should be magnetic. Some magnetic materials are intrinsically half-metallic, such as iron dihalide [14], transition-metal (TM) dihydride [15], TM dinitride [16], and Cr₃X₄ (X = S, Se, Te) [17], while the majority of them are not half-metallic.

With the rise of the two-dimensional (2D) materials, marked by the fabrication of graphene in 2004 [18], a lot of 2D

magnetic materials have been predicted and/or synthesized [19–26]. However, most of them are also non-half-metallic. A natural interesting question is whether they can be tuned to be half-metallic by certain external means. Fortunately, thus far, a few schemes have been proposed to realize half-metallicity in 2D materials. The first and most prominent example is zigzag-edge graphene nanoribbons (ZGNRs) in which half-metallicity is achieved by applying an external transverse electric field by Louie *et al.* [27]. Due to the energy degeneracy breaking of the spin resolved edge states in the two spin channels induced by the electrostatic potential energy drop along the electric field direction, both the valence band and conduction band in one spin channel will be shifted to the Fermi level while those of the other spin channel will shift far away from it simultaneously. Since the electrical field needs to be extremely strong to induce the half-metallicity, which is basically unavailable in laboratory, alternative methods have been proposed by many other groups. For example, Kan *et al.* proposed the edge decoration scheme to achieve half-metallicity in ZGNRs [28]. The -CH₃ group and -NO₂ group were used to saturate the dangling bonds of the edge carbon atoms on the different edges, which lower the local potential energy of one edge and increase it at the other edge, effectively generating a potential energy gradient between the

*Contact author: xzheng@njfu.edu.cn

†Contact author: hhao@hznu.edu.cn

two edges and inducing half-metallicity in the ZGNRs. Two other typical examples are contributed by Dutta *et al.*, [29] who replaced the central part of ZGNRs by BN nanoribbons (BNNRs), and by Zheng *et al.*, [30] who doped B atoms at one edge and N atoms at the other edge. The BN nanoribbon substitution scheme also causes potential difference along the transverse direction due to the asymmetry of BN nanoribbons, while the B-N codoping scheme at opposite edges directly control the depletion of electrons of the valence band edge state in one spin channel at one edge by B acceptor and the filling of electrons into the conduction band edge states localized at the other edge of the same spin channel by N donor due to their one more (N) or less (B) electron than the C atom. Based on the fact that the edge states of one spin channel is solely distributed at one carbon sublattice and those of the other spin channel are localized completely on the other carbon sublattice, Tao *et al.* proposed another scheme by AA stacking of a BN nanoribbon on the ZGNR, which generate a stagger potential energy distribution that increases the potential energy of one sublattice and decreases the potential energy of the other sublattice, ultimately shift the energy of the edge states of different spin channels towards opposite directions, and thus leading to a decreased band gap for one spin channel and an increased band gap for the other one. Then combined with photogalvanic effect, half-metallic transport is achieved in such a BNNR/ZGNR van der Waals (vdW) heterostructure [31].

The study of half-metallicity is then extended from the one dimensional ZGNRs to 2D materials that are periodic in the two in-plane directions. Stimulated by Louie *et al.*'s idea of applying a transverse electrical field to tune the energy of the electronic states localized at different spatial locations, Gong *et al.* realized half-metallicity in A-type antiferromagnetic bilayer VSe₂ system [32], in which the valence band states of the two spin channels are localized at different layers and those states in the conduction band are also localized at different layers. A vertical electrical field will play the same role as a transverse electrical field does in the ZGNRs, and thus half-metallicity is generated in the bilayer VSe₂. The same idea has also been applied to achieve half-metallicity in the A type antiferromagnetic bilayer LaBr₂ by Chen *et al.* [33]. However, all the schemes above are limited only to the antiferromagnetic systems where the examples mentioned previously such as ZGNRs [27], bilayer VSe₂ [28–32], and bilayer LaBr₂ [33] are all antiferromagnetic, with states of different spin channels distributed at different locations. For systems that are ferromagnetic and the states of different spin channels are not spatially separated, none of the schemes previously mentioned are applicable. How to achieve half-metallicity in such systems, especially in ferromagnetic monolayers, is both challenging and significant.

In this work, we propose a scheme to realize half-metallicity in a special type of ferromagnetic 2D materials called spin semiconductors. Spin semiconductors are ferromagnets characterized by the two bands right above and below the Fermi level coming from different spin channels and both bands are separated from all other bands above or below them by an energy gap [34]. Such kinds of ferromagnets are proved to be very useful in many fields, especially in pure spin current generation by thermoelectric effect [35] or photogal-

vanic effect [36]. Obviously, to get half-metallicity, we have to tune these bands to cross the Fermi level. Since the states from the spin up channel and spin down channels are evenly distributed in the whole systems, we can not use the methods that generate potential energy difference any more. However, a straightforward idea is to dope electrons or holes into the system, which may lead to partially filled valence band or conduction band. Since either the valence band or the conduction band takes only one spin channel, it will shift either the valence band or the conduction band to the Fermi level by either doping holes or doping electrons and finally makes it half-metallic. Such dopings can be implemented by stacking another 2D material on it to form vdW heterostructure. Due to the work function difference between the two contacted materials, charge transfer may occur. Either the amount or the direction of the charge transfer will be directly determined by the relative magnitudes of the work functions of the two materials. By taking the spin-semiconducting LaBr₂ monolayer [37,38] as an example, we intend to make it half-metallic based on charge transfer by stacking a ferroelectric 2D material α -In₂Se₃ onto it [39–41]. Since the ferroelectric 2D materials have different work functions on different sides as a result from the internal ferroelectric polarization, it will have more degree of freedom for charge transfer tuning, at least it can provide two different work functions and thus two possibilities of band alignment with that of LaBr₂ and the different contacts can be conveniently switched by the ferroelectric polarization reversal. Our density functional calculations indicate that half-metallicity can be generated in LaBr₂. More interestingly, half-metal and semiconductor will be exchanged upon the reversal of the ferroelectric polarization due to the different band alignment resulting from the different work function differences. Transport calculations in a multiferroic tunnel junction (MTJ) constructed from the LaBr₂/ α -In₂Se₃ vdW heterostructure demonstrate 99.94% spin polarization, giant tunnel electroresistance (TER) ratio ($2.11 \times 10^5\%$), and giant tunnel magnetoresistance (TMR) ratio ($1.62 \times 10^4\%$), realizing excellent performances in multiple purposes with the same functional material.

II. COMPUTATIONAL DETAILS

The structure relaxations and electronic structure calculations are performed by density functional theory as implemented in the Vienna *ab initio* Simulation Package (VASP) [42]. The exchange-correlation functional is described by the Perdew-Burke-Ernzerhof (PBE) form of the generalized gradient approximation (GGA) [43] and the projector-augmented plane wave potentials [44]. The fineness of the real-space grid is determined by the energy cutoff of 600 eV. A Hubbard U value of 5.5 eV is considered for the $4f$ orbitals of the La atoms to take into its correlation effect [45]. A $12 \times 12 \times 1$ Monkhorst-Pack k -point grid is chosen to sample the first Brillouin zone in the reciprocal space. The vacuum layer thickness is chosen as 15.0 Å. The van der Waals force was considered through the DFT-D2 method [46,47] in all the structural optimizations. The dipole correction has also been taken into account. The convergence criteria for force and total energy are chosen as 0.001 eV/Å and 10^{-8} eV, respectively.

The transport calculations are performed by the QUANTUMATK package [48–50], which combines density functional theory and nonequilibrium Green’s function, as implemented with linear combinations of atomic orbitals (LCAO). The exchange-correlation potential is described by GGA-PBE. Both the pseudopotentials and LCAO basis sets take the PseudoDojo form [49]. The k -point grid in the self-consistent calculation is set to $13 \times 1 \times 1$, whereas it is chosen as $100 \times 1 \times 1$ in the calculation of the transmission function since it demands a much denser k grid along the transverse periodic direction. The tunneling equilibrium conductance of the system is obtained by

$$G = G_0 \sum_{k_x} T(k_x, E), \quad (1)$$

where $T(k_x, E)$ is the transmission function of the electronic state at $k = k_x$ for energy E , and $G_0 = 2e^2/h$ is the conductance quanta. Further, the TER ratio of the system is calculated by [51]

$$\text{TER} = \frac{|G_{\uparrow} - G_{\downarrow}|}{\min(G_{\uparrow}, G_{\downarrow})} \times 100\%, \quad (2)$$

where G_{\uparrow} and G_{\downarrow} are the tunneling equilibrium conductance of the FTJ when the ferroelectric layer is in the polarization up (P_{\uparrow}) and polarization down (P_{\downarrow}) states, respectively. The TMR ratio is defined as [52]

$$\text{TMR} = \frac{G_P - G_{AP}}{G_{AP}} \times 100\%, \quad (3)$$

where G_P and G_{AP} are the tunneling equilibrium conductance of the magnetic tunnel junction in the parallel (P) magnetization and antiparallel (AP) magnetization states, respectively.

III. RESULTS AND DISCUSSION

A. Electronic structure of freestanding LaBr_2 and $\alpha\text{-In}_2\text{Se}_3$

First of all, before the formation of the vdW multiferroic heterostructure, the electronic structures of the free monolayer LaBr_2 and In_2Se_3 are revisited. The fully relaxed structures of them indicate that their primitive cells are both hexagonal, with the lattice constants as 4.09 Å and 4.11 Å, respectively, with the lattice mismatch between them as small as 0.4%. In the primitive cell, LaBr_2 includes one La atom and two Br atoms, while In_2Se_3 includes two In atoms and three Se atoms. The nearly perfect lattice commensuration between the two lattices makes them ideal for constructing vdW heterostructures, as shown in Fig. 1. The band structures of these two materials are shown in Figs. 2(a) and 2(b), respectively. Figure 2(a) indicates that LaBr_2 is a spin semiconductor, with the valence band contributed by spin up channel and the conduction band contributed by spin down channel. The spin gap defined by the distance between the spin up valence band maximum (VBM) and the spin down conduction band minimum (CBM) is 0.45 eV. In addition, the band gap of the spin up channel is 1.27 eV, while that for the spin down channel is 4.05 eV. Note that this is achieved with a U value of 5.5 eV for the $4f$ orbitals. Without U consideration, the flat $4f$ bands will lower down to mix with the spin down conduction band (not shown). More accurate calculations with hybrid functional HSE06 also indicate that the $4f$ orbitals should

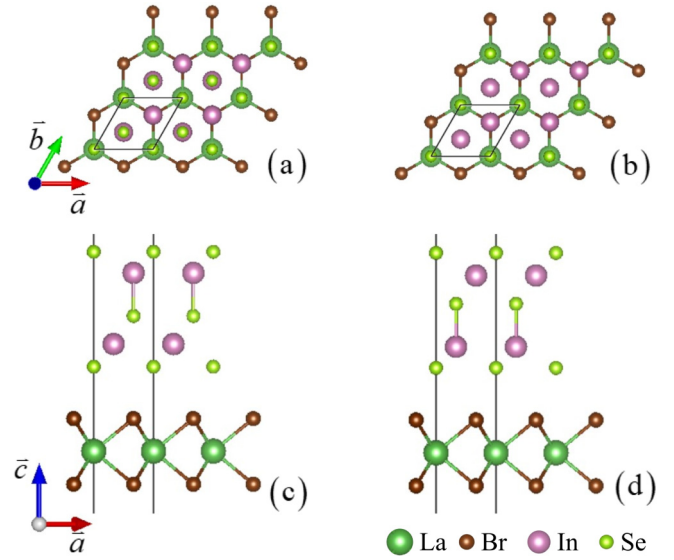


FIG. 1. The $\text{LaBr}_2/\alpha\text{-In}_2\text{Se}_3$ vdW heterostructure with the ferroelectric polarization: (a), (c) pointing up; (b), (d) pointing down. (a) and (b) are top views, while (c) and (d) are side views. The rhombus indicates the primitive cell.

be far above the spin down conduction band (beyond +3 eV) [38]. The PBE + U reproduces this feature well. Figure 2(b) indicates that In_2Se_3 is a semiconductor with an indirect band gap of 0.76 eV and its electrical dipole moment is obtained as $0.095 e \text{ \AA}/\text{unit cell}$. In_2Se_3 is a five-atomic-layer structure and the polarization reversal is switched by exchanging the central Se atom between two positions that are right below the upper layer In atom and right above the lower layer In atom in the unit cell [see Figs. 1(c) and 1(d)]. The magnetic moment of each La atom is $0.38 \mu_B$, but located in the interstitial region formed by three La atoms, a feature in line with the unique behavior of electride electrons, which is seen from the spin density shown in Figs. 2(c) and 2(d). These results are in good agreement with the literature [33,41].

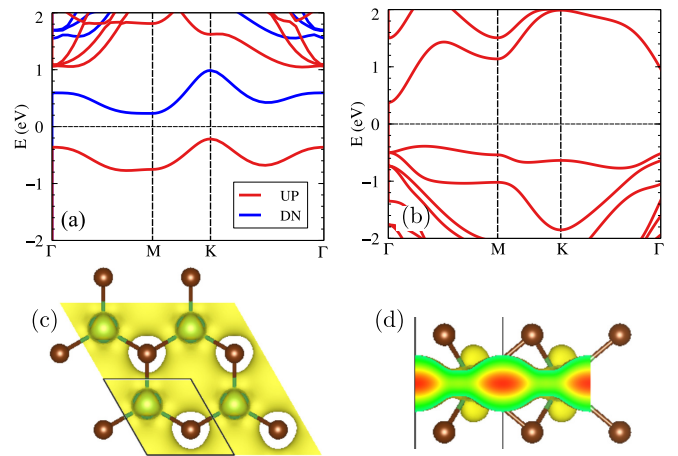


FIG. 2. The band structure of the isolated 2D material: (a) LaBr_2 ; (b) In_2Se_3 , UP stands for spin up and DN for spin down. The spin density of LaBr_2 : (c) top view; (d) side view, where the rhombus indicates a unit cell.

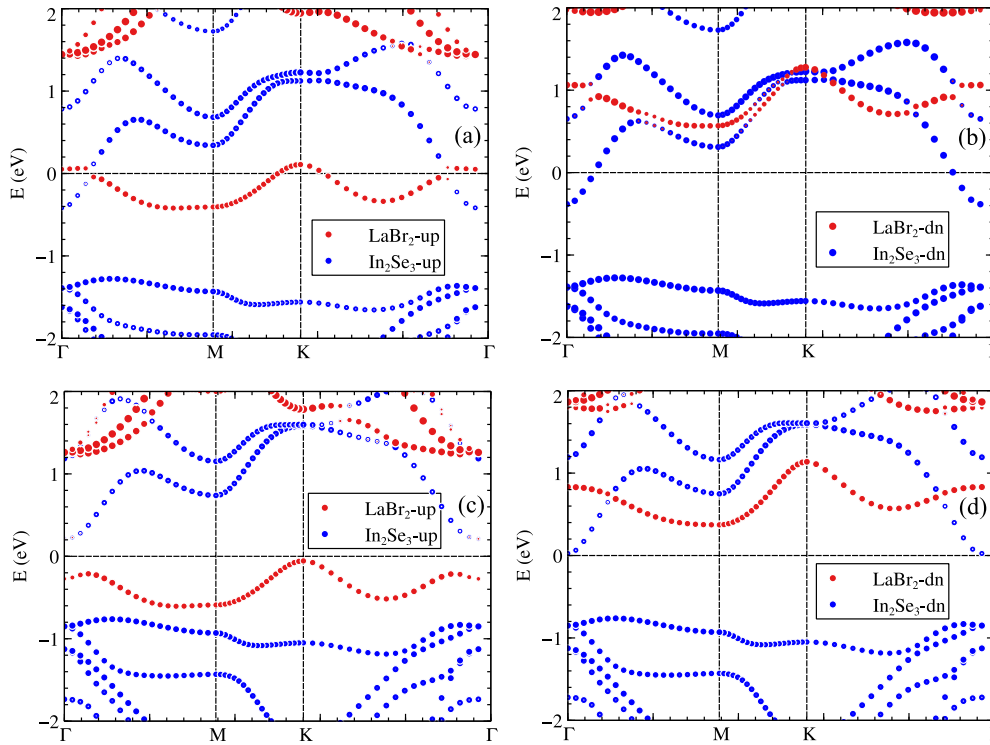


FIG. 3. The layer projected band structure of the $\text{LaBr}_2/\alpha\text{-In}_2\text{Se}_3$ vdW heterostructure: (a) and (b) for the P_\uparrow case while (c) and (d) for the P_\downarrow case, with up and dn standing for spin up and spin down, respectively.

B. Electronic structure of $\text{LaBr}_2/\alpha\text{-In}_2\text{Se}_3$ vdW heterostructure

After considering all possible stacking modes of the two materials, full relaxations reveal that the lowest-energy structure of the $\text{LaBr}_2/\alpha\text{-In}_2\text{Se}_3$ takes a common lattice constant of 4.09 Å, with the outmost Se atoms in In_2Se_3 right above the La atoms in LaBr_2 , which can be seen from the top view and side view in the polarization up and down cases shown in Figs. 1(a)–1(d). The interlayer distance between the LaBr_2 and In_2Se_3 is obtained as 3.081 Å, with the electrical dipole moment decreasing to $-0.02 e \text{Å}/\text{unit cell}$ in the polarization up (P_\uparrow) case and increasing to $0.12 e \text{Å}/\text{unit cell}$ in the polarization down (P_\downarrow) case. The great difference in the polarization strength in the two polarization states implies great changes in the electronic structure of the heterostructure accompanying with the polarization reversal. Such a change is first reflected in the layer-resolved band structure shown in Fig. 3. In the P_\uparrow case, the spin up VBM of LaBr_2 gets higher than the CBM of In_2Se_3 and the Fermi level crosses the two bands [see Fig. 3(a)]. However, the spin down conduction band of LaBr_2 is above the Fermi level [see Fig. 3(b)], thus LaBr_2 becomes half-metallic and In_2Se_3 becomes metallic. The metallicity in In_2Se_3 greatly decreases the polarization strength from 0.095 to $0.02 e \text{Å}/\text{unit cell}$ due to the screening effects of free electrons. In contrast, in the P_\downarrow case, both LaBr_2 and In_2Se_3 are insulators since there is a band gap for both materials. Therefore, with the ferroelectric polarization reversal, a metal to insulator transition occurs for both LaBr_2 and In_2Se_3 . Accordingly, the polarization strength slightly increases from 0.095 to $0.12 e \text{Å}/\text{unit cell}$. Obviously, from Fig. 3(a), the spin up valence band of LaBr_2 becomes partially unfilled while the conduction band of In_2Se_3 becomes

partially filled, which suggests there is charge transfer from LaBr_2 to In_2Se_3 . This is seen more clearly from the differential charge density as shown in Fig. 4. In both the P_\uparrow [Fig. 4(a)] and P_\downarrow [Fig. 4(b)] cases, there is charge depletion from inside of LaBr_2 to the interface region. The difference between the two cases is that, charge transfer from LaBr_2 goes inside In_2Se_3 in the P_\uparrow while it is not seen in the P_\downarrow [Fig. 4(b)] case. Conversely, it may be interpreted that it is

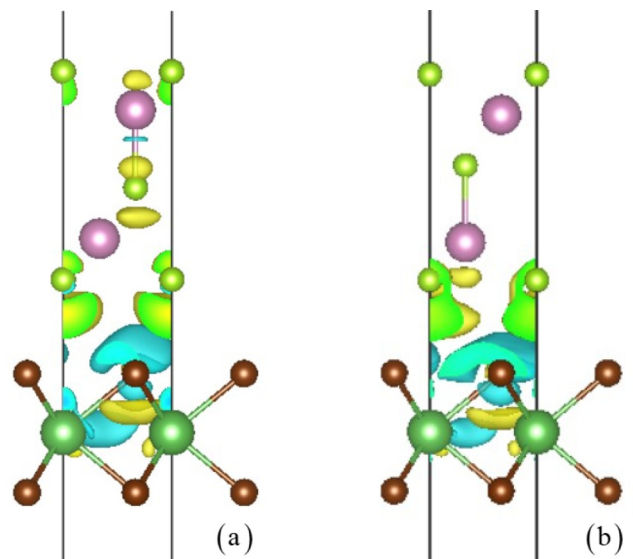


FIG. 4. The differential charge density of the $\text{LaBr}_2/\alpha\text{-In}_2\text{Se}_3$ vdW heterostructure in: (a) the P_\uparrow case; (b) the P_\downarrow case.

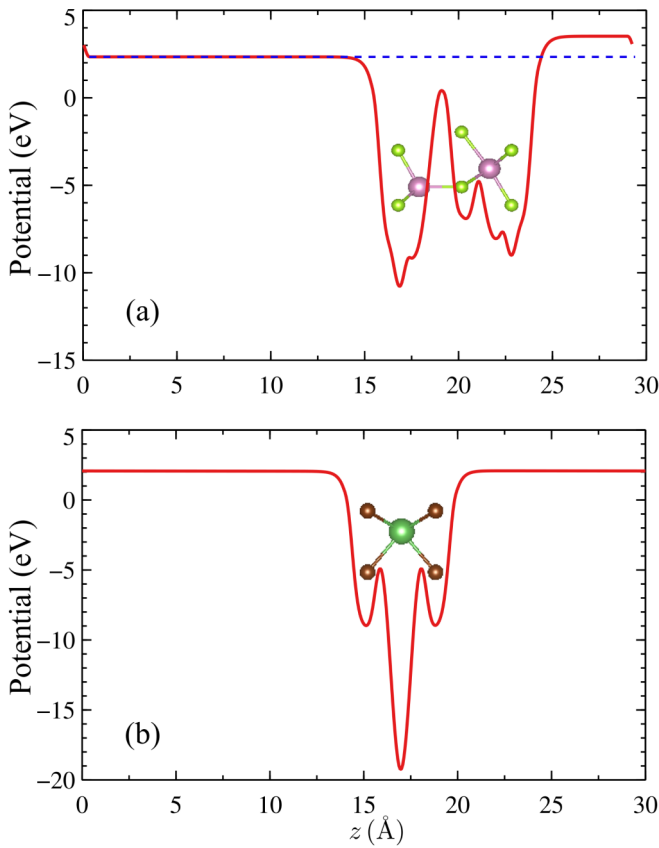


FIG. 5. The averaged electrostatic potential distribution along the vertical direction for: (a) In_2Se_3 ; (b) LaBr_2 .

the charge transfer that induces the metal-insulator transition. Then what is the origin of the charge transfer? It is well known that the work function measures the work that has to be done to take an electron from the Fermi level to the vacuum level. The relative work function difference will generate a contact potential difference, which acts as the driving force of charge transfer between two materials. Thus, next, the work functions of the two materials are studied. To get the vacuum level, the Hartree potential is averaged in the xy plane and its function as z along the vertical direction is calculated and shown in Fig. 5. It is found that the vacuum level of In_2Se_3 is different for both sides, with a potential energy drop of 1.18 eV, which leads to the two work functions of 5.20 eV and 6.38 eV for the two surfaces. Note that in the calculation of work functions with $W = E_{\text{vac}} - E_F$, although for intrinsic semiconductors or insulators the Fermi level is not well defined, it is reasonable to take it as the VBM for the ground state [41,53,54]. For LaBr_2 , for each spin channel, there will be a work function due to their different VBM. The work function for spin up channel is 4.20 eV, while that for the spin down channel is 7.80 eV. All these work functions lead to the initial band alignments as shown in Fig. 6. When the P_- side of In_2Se_3 [negative charge side of the dipole, also the higher potential energy side and the higher work function side, marked by “ $\text{In}_2\text{Se}_3(-)$ ” in Fig. 6] is contacted with LaBr_2 , the band alignment between spin up of LaBr_2 and In_2Se_3 belongs to type III, which leads to charge transfer from the spin up VBM of LaBr_2 to the CBM of In_2Se_3 and the transfer amount is rather large. In the meantime, the

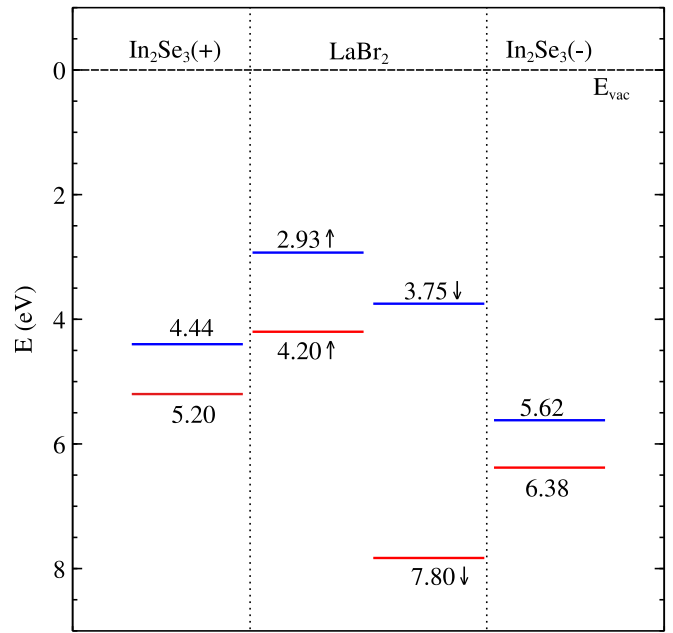


FIG. 6. The initial band alignments of the vdW heterostructure. The horizontal dashed line indicates the vacuum level, the blue solid line indicates the CBM, while the red solid line indicates the VBM, which also marks the work function since for insulators, the work function is calculated by the difference of vacuum level and the VBM at zero temperature. The arrows indicate spin up and spin down channels in LaBr_2 .

spin down channel of LaBr_2 forms a type I band alignment with In_2Se_3 , thus there is no charge transfer between them. The band alignments of the two spin channels finally lead to the spin up valence band of LaBr_2 becoming partially filled and LaBr_2 becomes half-metallic. When the P_+ side [marked by “ $\text{In}_2\text{Se}_3(+)$ ” in Fig. 6] of In_2Se_3 is contacted with LaBr_2 , we find that the spin down channel of LaBr_2 still forms the type-I initial band alignment with In_2Se_3 , which leads to no charge transfer between them. The spin up channel forms with type-III band alignment with In_2Se_3 , which ideally should lead to charge transfer between them. However, the spin up VBM of LaBr_2 is only slightly (0.24 eV) above the In_2Se_3 CBM. Due to the large interface tunnel barrier, the charge transfer is negligibly small. That is why LaBr_2 and In_2Se_3 are both insulators. Nevertheless, the spin up VBM of LaBr_2 and spin down CBM of In_2Se_3 get very close. Interestingly, for In_2Se_3 , the spin up CBM is higher than the spin down CBM, which leads to spin splitting of LaBr_2 .

C. Transport properties in $\text{LaBr}_2/\alpha\text{-In}_2\text{Se}_3$ vdW MTJ

Although LaBr_2 becomes half-metallic in the P_\uparrow case, how to utilize the half-metallicity in it is an important question to ask since the vdW heterostructure as a whole is not half-metallic and the projected bands of LaBr_2 and In_2Se_3 are mixed around the Fermi level. In order to utilize the half-metallicity in LaBr_2 , we construct a multiferroic tunnel junction as shown in Fig. 7, which has $\text{LaBr}_2/\alpha\text{-In}_2\text{Se}_3$ as the leads and LaBr_2 as the channel region, with LaBr_2 of the three regions as a whole sheet. Both the leads and the central region

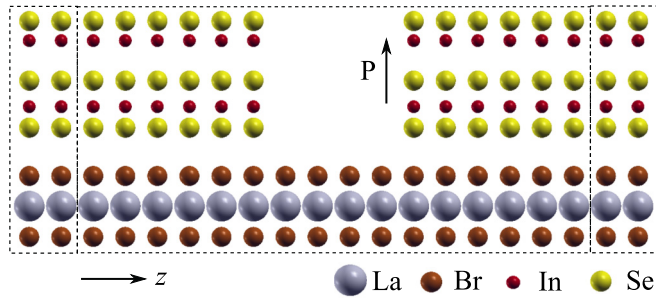


FIG. 7. The structure of the multiferroic tunnel junction constructed with the $\text{LaBr}_2/\alpha\text{-In}_2\text{Se}_3$ vdW heterostructure. Transport is along the z direction.

are composed by periodically repeating the smallest rectangular supercell, which is about 7.080 \AA in the x direction and 4.088 \AA in z (transport) direction, as marked by the left and right dashed line box in Fig. 7. The central region includes two supercells of LaBr_2 as the channel region and three supercells of $\text{LaBr}_2/\alpha\text{-In}_2\text{Se}_3$ vdW heterostructure in both the left and right buffer layers. Figure 7 shows the case with the P_\uparrow ferroelectric polarization case, with the polarization revertible by an opposite electric field. In addition, we may apply different magnetic fields to control the parallel or antiparallel magnetization directions of the two leads. Thus, we may realize tunnel electroresistance and tunnel magnetoresistance in this same MTJ. We care how much the TER ratio and the TMR ratio will be achieved. Our transport calculations are performed with PBE functional, namely, without considering U . This is reasonable since we have compared the band structures with and without U (not shown) and we get basically the same band structure in the energy range below $+1 \text{ eV}$, while the electron transport properties are determined only by the electrons nearby the Fermi level.

First, we study the case with uniform magnetization in LaBr_2 under different ferroelectric polarization directions of In_2Se_3 . The transmission functions of the P_\downarrow and the P_\uparrow cases are given in Figs. 8(a) and 8(b), respectively. We find that there are a wide spin up transmission peak below the Fermi level and a wide spin down transmission peak above the Fermi level [Fig. 8(a)]. These two peaks actually arise from the LaBr_2 spin semiconducting bands since the Bloch

states from the In_2Se_3 are almost completely blocked due to the vacuum gap between the two leads. However, around the Fermi level, there is a transmission gap, which is consistent with band gap in Figs. 3(c) and 3(d). It means it lies in a poorly conducting state. Note the appearance of a small spin up peak in Fig. 8(a) right above the Fermi level. Due to the In_2Se_3 channel being blocked by the gap, there should be no spin up contribution above the Fermi energy up to 1 eV . However, if we inspect the layer-projected band structure carefully, we will see some contribution from LaBr_2 around the CBM in the spin up channel [see Fig. 3(c)]. This is due to orbital hybridization between LaBr_2 and In_2Se_3 . This can be seen from the charge accumulation at the interface as seen in Fig. 4(b). From Fig. 3(c), we also see that, when approaching the Γ point along the spin down conduction band, the weight of In_2Se_3 gets increasingly smaller while that of the spin up channel of LaBr_2 gets bigger. Thus, we believe that the spin up transmission contribution above the Fermi level in Fig. 8(a) should originate from this hybridization induced spin up LaBr_2 states.

On the contrary, in the P_\uparrow case, a wide spin up transmission peak crosses the Fermi level. Thus, half-metallic transport is realized. We get at the Fermi level $T_{\text{up}} = 3.7944 \times 10^{-1}$ and $T_{\text{dn}} = 1.1395 \times 10^{-4}$ in the P_\uparrow case and $T_{\text{up}} = 7.3997 \times 10^{-5}$ and $T_{\text{dn}} = 1.0580 \times 10^{-4}$ in the P_\downarrow , which leads to spin polarization as high as 99.94% in the P_\uparrow state and a TER ratio of $2.11 \times 10^5\%$ in the MTJ. In the conducting P_\uparrow case, when we revert the magnetization of the right lead with a magnetic field to have antiparallel magnetic configuration, we will see that in the energy range studied, the transmissions are almost completely suppressed, especially around the Fermi level. We get an actual transmission at the Fermi level of $T_{\text{dn}} = 4.2041 \times 10^{-4}$ and $T_{\text{dn}} = 1.9060 \times 10^{-3}$ for the spin up and spin down channels, respectively. Combined with the P_\uparrow case in parallel magnetic configuration, we will get a giant TMR ratio of $1.62 \times 10^4\%$. This can be understood as follows. With reversal of the magnetization of the right lead, the spin indices of the LaBr_2 in both leads are exchanged. Due to spin mismatching in LaBr_2 and almost complete blocking in the In_2Se_3 due to the existence of the gap, the transmission around the Fermi level will become negligible in the AP case, leading to an extremely low conductance state.

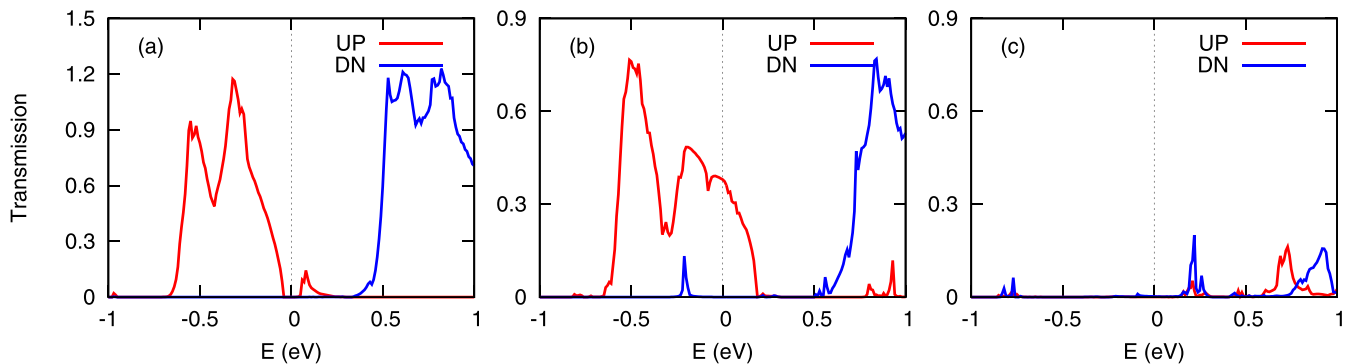


FIG. 8. The transmission function of the MTJ in: (a) P_\downarrow polarization and P magnetization configuration; (b) P_\uparrow polarization and P magnetization configuration; (c) P_\uparrow polarization and AP magnetization configuration.

IV. CONCLUSION

In summary, by taking LaBr_2 as an example, we have proposed a scheme to realize electron half-metallicity in 2D spin-semiconducting ferromagnetic materials by stacking a 2D ferroelectric material with out-of-plane ferroelectric polarization. This scheme works with charge transfer due to work function differences of the contacted surfaces of the two materials. No matter whether the magnetic material receives electrons or loses electrons, half-metallicity will be achieved. The key requirement is that the two contacted materials have type-III initial band alignment, where work functions of the materials are the most important physical quantity to consider. In our example, LaBr_2 loses electrons so that the spin up valence band becomes partially filled in the P_{\uparrow} case and thus becomes half-metallic. Interestingly, with the ferroelectric polarization reversal, LaBr_2 will recover semiconductor again. Such a switching can lead to interesting transport behaviors. In the multiferroic tunnel junction constructed with $\text{LaBr}_2/\alpha\text{-In}_2\text{Se}_3$ vdW heterostructure, 99.94% spin

polarization equilibrium conductance, $2.11 \times 10^5\%$ tunnel electroresistance ratio and $1.62 \times 10^4\%$ tunnel magnetoresistance ratio are observed. For other spin semiconductors, by proper choice of the stacked 2D ferroelectric material with appropriate ferroelectric polarization and work functions, spin up half-metal, spin down half-metal, or bipolar half-metal can be achieved due to the ferroelectric polarization reversal under external electric field. The findings suggest a novel scheme for designing high performance multifunctional multiferroic tunnel junctions based on ferromagnetic spin semiconductors.

ACKNOWLEDGMENTS

We gratefully acknowledge the support from the National Natural Science Foundation of China (Grants No. 12074230, No. 12474047, and No. 11974355), the Fund for Shanxi “1331 Project,” and Research Project Supported by Shanxi Scholarship Council of China.

-
- [1] M. N. Baibich, J. M. Broto, A. Fert, F. N. V. Dau, F. Petroff, P. Etienne, G. Creuzet, A. Friederich, and J. Chazelas, Giant magnetoresistance of (001)Fe/(001)Cr magnetic superlattices, *Phys. Rev. Lett.* **61**, 2472 (1988).
- [2] G. Binasch, P. Grunberg, F. Saurenbach, and W. Zinn, Enhanced magnetoresistance in layered magnetic structures with antiferromagnetic interlayer exchange, *Phys. Rev. B* **39**, 4828 (1989).
- [3] I. Žutić, J. Fabian, and S. Das Sarma, Spintronics: Fundamentals and applications, *Rev. Mod. Phys.* **76**, 323 (2004).
- [4] B. Dieny, I. L. Prejbeanu, K. Garello, P. Gambardella, P. Freitas, R. Lehnendorff, W. Raberg, U. Ebels, S. O. Demokritov, J. Akerman, A. Deac, P. Pirro, C. Adelmann, A. Anane, A. V. Chumak, A. Hirohata, S. Mangin, S. O. Valenzuela, M. C. Onbaşı, M. d’Aquino *et al.*, Opportunities and challenges for spintronics in the microelectronics industry, *Nat. Electron.* **3**, 446 (2020).
- [5] V. Baltz, A. Manchon, M. Tsoi, T. Moriyama, T. Ono, and Y. Tserkovnyak, Antiferromagnetic spintronics, *Rev. Mod. Phys.* **90**, 015005 (2018).
- [6] S. K. Kim, G. S. D. Beach, K.-J. Lee, T. Ono, T. Rasing, and H. Yang, Ferrimagnetic spintronics, *Nat. Mater.* **21**, 24 (2022).
- [7] S. A. Wolf, D. D. Awschalom, R. A. Buhrman, J. M. Daughton, S. von Molnar, M. L. Roukes, A. Y. Chtchelkanova, and D. M. Treger, Spintronics: A spin-based electronics vision for the future, *Science* **294**, 1488 (2001).
- [8] F. Pulizzi, Spintronics, *Nat. Mater.* **11**, 367 (2012).
- [9] D. D. Awschalom and M. E. Flatté, Challenges for semiconductor spintronics, *Nat. Phys.* **3**, 153 (2007).
- [10] R. A. de Groot, F. M. Mueller, P. G. van Engen, and K. H. J. Buschow, New class of materials: Half-metallic ferromagnets, *Phys. Rev. Lett.* **50**, 2024 (1983).
- [11] J.-H. Park, E. Vescovo, H.-J. Kim, C. Kwon, R. Ramesh, and T. Venkatesan, Direct evidence for a half-metallic ferromagnet, *Nature (London)* **392**, 794 (1998).
- [12] S. S. Mallajosyula and S. K. Pati, Vanadium-benzimidazole-modified sDNA: A one-dimensional half-metallic ferromagnet, *J. Phys. Chem. B* **111**, 13877 (2007).
- [13] V. V. Maslyuk, A. Bagrets, V. Meded, A. Arnold, F. Evers, M. Brandbyge, T. Bredow, and I. Mertig, Organometallic benzene-vanadium wire: A one-dimensional half-metallic ferromagnet, *Phys. Rev. Lett.* **97**, 097201 (2006).
- [14] M. Ashton, D. Gluhovic, S. B. Sinnott, J. Guo, D. A. Stewart, and R. G. Hennig, Two-dimensional intrinsic half-metals with large spin gaps, *Nano Lett.* **17**, 5251 (2017).
- [15] Q. Wu, Y. Zhang, Q. Zhou, J. Wang, and X. C. Zeng, Transition-metal dihydride monolayers: A new family of two-dimensional ferromagnetic materials with intrinsic room-temperature half-metallicity, *J. Phys. Chem. Lett.* **9**, 4260 (2018).
- [16] Z. Liu, J. Liu, and J. Zhao, YN2 monolayer: Novel p-state Dirac half metal for high-speed spintronics, *Nano Res.* **10**, 1972 (2017).
- [17] F. Zhang, Z. Wang, J. Dong, A. Nie, J. Xiang, W. Zhu, Z. Liu, and C. Tao, Atomic-scale observation of reversible thermally driven phase transformation in 2D In_2Se_3 , *ACS Nano* **13**, 8004 (2019).
- [18] K. S. Novoselov, A. K. Geim, S. V. Morozov, D. Jiang, Y. Zhang, S. V. Dubonos, I. V. Grigorieva, and A. A. Firsov, Electric field effect in atomically thin carbon films, *Science* **306**, 666 (2004).
- [19] N. Sivasdas, M. W. Daniels, R. H. Swendsen, S. Okamoto, and D. Xiao, Magnetic ground state of semiconducting transition-metal trichalcogenide monolayers, *Phys. Rev. B* **91**, 235425 (2015).
- [20] H. Wang, F. Fan, S. Zhu, and H. Wu, Doping enhanced ferromagnetism and induced half-metallicity in CrI_3 monolayer, *Europhys. Lett.* **114**, 47001 (2016).
- [21] C. Gong, L. Li, Z. Li, H. Ji, A. Stern, Y. Xia, T. Cao, W. Bao, C. Wang, Y. Wang, Z. Q. Qiu, R. J. Cava, S. G. Louie, J. Xia, and X. Zhang, Discovery of intrinsic ferromagnetism in

- two-dimensional van der Waals crystals, *Nature (London)* **546**, 265 (2017).
- [22] B. Huang, G. Clark, E. Navarro-Moratalla, D. R. Klein, R. Cheng, K. L. Seyler, D. Zhong, E. Schmidgall, M. A. McGuire, D. H. Cobden, W. Yao, D. Xiao, P. Jarillo-Herrero, and X. Xu, Layer-dependent ferromagnetism in a van der Waals crystal down to the monolayer limit, *Nature (London)* **546**, 270 (2017).
- [23] J. Feng, X. Sun, C. Wu, L. Peng, C. Lin, S. Hu, J. Yang, and Y. Xie, Metallic few-layered VS₂ ultrathin nanosheets: High two-dimensional conductivity for in-plane supercapacitors, *J. Am. Chem. Soc.* **133**, 17832 (2011).
- [24] M. Bonilla, S. Kolekar, Y. Ma, H. C. Diaz, V. Kalappattil, R. Das, T. Eggers, H. R. Gutierrez, M.-H. Phan, and M. Batzill, Strong room-temperature ferromagnetism in VSe₂ monolayers on van der Waals substrates, *Nature Nanotechnol.* **13**, 289 (2018).
- [25] P. Jiang, L. Kang, X. Zheng, Z. Zeng, and S. Sanvito, Computational prediction of a two-dimensional semiconductor SnO₂ with negative Poisson's ratio and tunable magnetism by doping, *Phys. Rev. B* **102**, 195408 (2020).
- [26] J.-J. He, F.-W. Guo, H.-M. Ni, J.-B. Dong, W.-D. Cui, T.-Y. Lu, J.-R. Yuan, Y.-D. Guo, and X.-H. Yan, Modulation of edge defects on dual-spin filtering in zigzag β -SiC₇ nanoribbons, *J. Chem. Phys.* **158**, 204105 (2023).
- [27] Y.-W. Son, M. L. Cohen, and S. G. Louie, Half-metallic graphene nanoribbons, *Nature (London)* **444**, 347 (2006).
- [28] E.-j. Kan, Z. Li, J. Yang, and J. G. Hou, Half-metallicity in edge-modified zigzag graphene nanoribbons, *J. Am. Chem. Soc.* **130**, 4224 (2008).
- [29] S. Dutta, A. K. Manna, and S. K. Pati, Intrinsic half-metallicity in modified graphene nanoribbons, *Phys. Rev. Lett.* **102**, 096601 (2009).
- [30] X. H. Zheng, X. L. Wang, T. A. Abteu, and Z. Zeng, Building half-metallicity in graphene nanoribbons by direct control over edge states occupation, *J. Phys. Chem. C* **114**, 4190 (2010).
- [31] X. Tao, L. Zhang, X. Zheng, H. Hao, X. Wang, L. Song, Z. Zeng, and H. Guo, h-BN/graphene van der Waals vertical heterostructure: a fully spin-polarized photocurrent generator, *Nanoscale* **10**, 174 (2018).
- [32] S.-J. Gong, C. Gong, Y.-Y. Sun, W.-Y. Tong, C.-G. Duan, J.-H. Chu, and X. Zhang, Electrically induced 2D half-metallic anti-ferromagnets and spin field effect transistors, *Proc. Natl. Acad. Sci.* **115**, 8511 (2018).
- [33] Q. Chen, X. Zheng, P. Jiang, Y.-H. Zhou, L. Zhang, and Z. Zeng, Electric field induced tunable half-metallicity in an a-type antiferromagnetic bilayer LaBr₂, *Phys. Rev. B* **106**, 245423 (2022).
- [34] Z. F. Wang, S. Jin, and F. Liu, Spatially separated spin carriers in spin-semiconducting graphene nanoribbons, *Phys. Rev. Lett.* **111**, 096803 (2013).
- [35] X. Chen, Y. Liu, B.-L. Gu, W. Duan, and F. Liu, Giant room-temperature spin caloritronics in spin-semiconducting graphene nanoribbons, *Phys. Rev. B* **90**, 121403(R) (2014).
- [36] X. Tao, P. Jiang, H. Hao, X. Zheng, L. Zhang, and Z. Zeng, Pure spin current generation via photogalvanic effect with spatial inversion symmetry, *Phys. Rev. B* **102**, 081402(R) (2020).
- [37] J. Zhou, Y. P. Feng, and L. Shen, Atomic-orbital-free intrinsic ferromagnetism in electrenes, *Phys. Rev. B* **102**, 180407(R) (2020).
- [38] P. Zhao, Y. Ma, C. Lei, H. Wang, B. Huang, and Y. Dai, Single-layer LaBr₂: Two-dimensional valleytronic semiconductor with spontaneous spin and valley polarizations, *Appl. Phys. Lett.* **115**, 261605 (2019).
- [39] W. Ding, J. Zhu, Z. Wang, Y. Gao, D. Xiao, Y. Gu, Z. Zhang, and W. Zhu, Prediction of intrinsic two-dimensional ferroelectrics in In₂Se₃ and other III₂-VI₃ van der Waals materials, *Nature Commun.* **8**, 14956 (2017).
- [40] S. Wan, Y. Li, W. Li, X. Mao, C. Wang, C. Chen, J. Dong, A. Nie, J. Xiang, Z. Liu, W. Zhu, and H. Zeng, Nonvolatile ferroelectric memory effect in ultrathin α -In₂Se₃, *Adv. Funct. Mater.* **29**, 1808606 (2019).
- [41] L. Kang, P. Jiang, H. Hao, Y. Zhou, X. Zheng, L. Zhang, and Z. Zeng, Giant tunneling electroresistance in two-dimensional ferroelectric tunnel junctions with out-of-plane ferroelectric polarization, *Phys. Rev. B* **101**, 014105 (2020).
- [42] G. Kresse and J. Furthmüller, Efficient iterative schemes for *ab initio* total-energy calculations using a plane-wave basis set, *Phys. Rev. B* **54**, 11169 (1996).
- [43] J. P. Perdew, K. Burke, and M. Ernzerhof, Generalized gradient approximation made simple, *Phys. Rev. Lett.* **77**, 3865 (1996).
- [44] P. E. Blochl, Projector augmented-wave method, *Phys. Rev. B* **50**, 17953 (1994).
- [45] M. Topsakal and R. Wentzcovitch, Accurate projected augmented wave (PAW) datasets for rare-earth elements (RE=La-Lu), *Comput. Mater. Sci.* **95**, 263 (2014).
- [46] S. Grimme, Semiempirical GGA-type density functional constructed with a long-range dispersion correction, *J. Comput. Chem.* **27**, 1787 (2006).
- [47] T. Bučko, J. Hafner, S. Lebègue, and J. G. Ángyán, Improved description of the structure of molecular and layered crystals: *Ab Initio* DFT calculations with van der Waals corrections, *J. Phys. Chem. A* **114**, 11814 (2010).
- [48] S. Smidstrup, T. Markussen, P. Vancraeyveld, J. Wellendorff, J. Schneider, T. Gunst, B. Verstichel, D. Stradi, P. A. Khomyakov, U. G. Vej-Hansen, M.-E. Lee, S. T. Chill, F. Rasmussen, G. Penazzi, F. Corsetti, A. Ojanperä, K. Jensen, M. L. N. Palsgaard, U. Martinez, A. Blom *et al.*, QuantumATK: an integrated platform of electronic and atomic-scale modelling tools, *J. Phys.: Condens. Matter* **32**, 015901 (2020).
- [49] M. van Setten, M. Giantomassi, E. Bousquet, M. Verstraete, D. Hamann, X. Gonze, and G.-M. Rignanese, The pseudodojo: Training and grading a 85 element optimized norm-conserving pseudopotential table, *Comput. Phys. Commun.* **226**, 39 (2018).
- [50] M. Brandbyge, J.-L. Mozos, P. Ordejón, J. Taylor, and K. Stokbro, Density-functional method for nonequilibrium electron transport, *Phys. Rev. B* **65**, 165401 (2002).
- [51] L. L. Tao and J. Wang, Ferroelectricity and tunneling electroresistance effect driven by asymmetric polar interfaces in all-oxide ferroelectric tunnel junctions, *Appl. Phys. Lett.* **108**, 062903 (2016).
- [52] E. Y. Tsymal, O. N. Mryasov, and P. R. LeClair, Spin-dependent tunnelling in magnetic tunnel junctions, *J. Phys.: Condens. Matter* **15**, R109 (2003).

- [53] L. Kang, P. Jiang, H. Hao, Y. Zhou, X. Zheng, L. Zhang, and Z. Zeng, Giant tunnel electroresistance in ferroelectric tunnel junctions with metal contacts to two-dimensional ferroelectric materials, *Phys. Rev. B* **103**, 125414 (2021).
- [54] A. Xie, H. Hao, C.-S. Liu, X. Zheng, L. Zhang, and Z. Zeng, Giant tunnel electroresistance in two-dimensional ferroelectric tunnel junctions constructed with a $\text{Sc}_2\text{CO}_2/\text{In}_2\text{Se}_3$ van der Waals ferroelectric heterostructure, *Phys. Rev. B* **107**, 115427 (2023).